Suppression of Collisional Shifts in a Strongly Interacting Lattice Clock

Matthew D. Swallows, *et al.*

Science **331**, 1043 (2011);
DOI: 10.1126/science.1196442

Suppression of Collisional Shifts in a Strongly Interacting Lattice Clock

Matthew D. Swallows,[1] Michael Bishof,[1] Yige Lin,[1,2] Sebastian Blatt,[1] Michael J. Martin,[1] Ana Maria Rey,[1] Jun Ye[1]*

Optical lattice clocks with extremely stable frequency are possible when many atoms are interrogated simultaneously, but this precision may come at the cost of systematic inaccuracy resulting from atomic interactions. Density-dependent frequency shifts can occur even in a clock that uses fermionic atoms if they are subject to inhomogeneous optical excitation. However, sufficiently strong interactions can suppress collisional shifts in lattice sites containing more than one atom. We demonstrated the effectiveness of this approach with a strontium lattice clock by reducing both the collisional frequency shift and its uncertainty to the level of 10^{-17}. This result eliminates the compromise between precision and accuracy in a many-particle system; both will continue to improve as the number of particles increases.

Strongly interacting quantum systems can exhibit counterintuitive behaviors. For example, frequency shifts of a microwave transition in a quantum gas remain finite close to a Feshbach resonance (*1*–*3*). In particular, the effective interaction strength is enhanced in low-dimensional systems, resulting in particles that avoid each other so as to minimize their total energy. This tendency can lead to behavior that in many respects resembles that of noninteracting systems. One such example is the Tonks-Girardeau regime of an ultracold Bose gas, in which the strong repulsion between particles mimics the Pauli exclusion principle, causing the bosons to behave like noninteracting fermions (*4*–*7*). Here we show that the enhancement of atomic interactions in a strongly interacting, effectively one-dimensional (1D) fermionic system suppresses collisional frequency shifts in an optical atomic clock.

A primary systematic effect of state-of-the-art optical lattice clocks is the density-dependent frequency shift (*8*, *9*). This shift arises from collisions between fermionic atoms that are subject to slightly inhomogeneous optical excitations (*10*, *11*); several theories of the shift mechanism have been proposed (*12*–*14*). By tightly confining atoms in an array of quasi-1D potentials formed by a 2D optical lattice, we increase the strength of atomic interactions to the point where the thermally averaged mean interaction energy per particle becomes the largest relevant energy scale other than the temperature, making the system strongly interacting in effect. In this regime, collisions are suppressed because evolution into a many-particle state in which *s*-wave scattering can occur is energetically unfavorable. This mechanism was first suggested in (*13*).

Collisional frequency shifts could also be suppressed by confining atoms in a 3D lattice with filling factor less than or equal to 1 per lattice site. However, vector and tensor shifts of the optical clock transition are a serious concern with a 3D fermionic lattice clock (*15*). A 3D lattice clock using bosonic ^{88}Sr has been demonstrated (*16*), and its collisional shift was characterized at the level of 7×10^{-16}, but the state-mixing techniques that are used to enable the $^1S_0 \rightarrow {}^3P_0$ clock transition in bosonic isotopes result in sizable systematic shifts of the clock frequency that must be carefully controlled. The work presented here will allow operation of a fermionic lattice clock with a filling factor much greater than 1 and a greatly reduced sensitivity to collisional effects.

To gain insight into the origin of the collisional frequency shift and the interaction-induced suppression, we consider a model system: two fermionic atoms, each of whose electronic degrees of freedom form a two-level, pseudospin-½ system ($|g\rangle$ and $|e\rangle$), confined in a 1D harmonic oscillator potential [for a full many-body treatment of an arbitrary number of atoms, see (*17*)]. The collective pseudospin states of these two identical fermions can be expressed with a basis comprising three pseudospin-symmetric triplet states and an antisymmetric singlet state (*12*, *13*). Because the atoms are initially prepared in the same internal state ($|g\rangle$), with their internal degrees of freedom symmetric with respect to exchange, the Pauli exclusion principle requires that their spatial wave function be antisymmetric and thus they experience no *s*-wave interactions. If the atoms are coherently driven with the same Rabi frequency $\overline{\Omega} = (\Omega_{n_1} + \Omega_{n_2})/2 = \Omega_{n_1}$, their electronic degrees of freedom remain symmetric under exchange. Here, n_i represents axial vibrational modes in each 1D tube-shaped optical trap, and Ω_{n_i} is the mode-dependent Rabi frequency, which is proportional to the bare Rabi frequency Ω_0^B. Consequently, these atoms will not experience any *s*-wave interactions during the excitation of the clock transition. However, if $\Delta\Omega = (|\Omega_{n_1} - \Omega_{n_2}|)/2$ is not zero, the optical excitation inhomogeneity can transfer atoms with a certain probability to the antisymmetric spin state (singlet) that is separated from the triplet states by an interaction energy U, because in the singlet state the atoms do interact. U, which is inversely proportional to the atomic confinement volume, gives rise to a frequency shift during clock interrogation (*12*, *13*).

Figure 1 contrasts the current 2D lattice experiment with prior studies carried out in a 1D lattice (*10*, *11*). In a 1D lattice, U is typically smaller than $2\,\overline{\Omega}$ (the energy spread of the driven triplet states at zero detuning). Consequently, any small excitation inhomogeneity $\Delta\Omega$ can efficiently populate the singlet state. By tightly confining atoms in a 2D lattice, one can reach the limit where $U >> \overline{\Omega}$, inhibiting the evolution into the singlet state; as a result, the collisional frequency shift of the clock transition is suppressed. In this

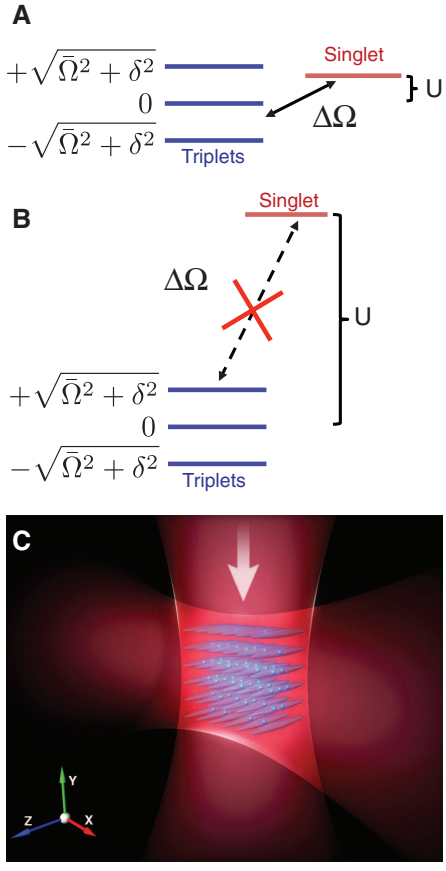

Fig. 1. A schematic of the interaction blockade mechanism responsible for the suppression of collisional frequency shifts. (**A**) In a 1D optical lattice, the interaction energy of the singlet state lies within the energies of the dressed triplet states (characterized by an energy spread on the order of $\overline{\Omega}$). A weak excitation inhomogeneity characterized by $\Delta\Omega$ is capable of producing triplet-singlet mixtures, causing a collisional frequency shift proportional to the interaction strength U. (**B**) In a 2D optical lattice, the interaction energy exceeds the atom-light Rabi frequency, creating an energy gap between the spin triplet and singlet states. Evolution into the singlet state is inhibited, and the collisional frequency shift is suppressed. (**C**) Quasi-1D tube-like optical potentials formed by two intersecting optical lattices. The laser that interrogates the clock transition propagates along $\hat{Y}$, the vertical axis.

[1]JILA, National Institute of Standards and Technology, and Department of Physics, University of Colorado, Boulder, CO 80309, USA. [2]National Institute of Metrology, Beijing 100013, China.

*To whom correspondence should be addressed. E-mail: ye@jila.colorado.edu

regime, the singlet state can only participate as a "virtual" state in second-order excitation processes and the frequency shift scales as $\Delta\Omega^2/U$. Such behavior is reminiscent of the dipolar blockade mechanism in a Rydberg atom gas (*18*). In effect, the singlet resonance has been shifted so far from the triplet resonances that it is completely resolved from them, and any associated line pulling is negligible.

This simple spin model can be extended to the finite temperature regime with a thermal average over vibrational modes n_i. Figure 2 shows the calculated fractional frequency shift as a function of the temperature-independent interaction parameter $u = 4\omega_\perp(a_{eg}^-/a_{ho})$ [u is related to the thermally averaged quantity U; see (*17*) for detailed derivations]. Here, $\omega_\perp = \sqrt{\omega_X\omega_Y}$ is the geometric mean of the transverse trapping frequencies, a_{eg}^- is the singlet g-e scattering length, and a_{ho} is the harmonic oscillator length along $\hat{Z}$. The suppression becomes less effective if Ω_0^B becomes comparable to u, or when $\Delta\Omega_{\vec{n}}$ increases at larger temperatures. These considerations imply that clock experiments based on Ramsey interrogation will not easily satisfy the suppression conditions outlined here, because the short pulses applied in the Ramsey scheme generally have a Rabi frequency much larger than those used in Rabi spectroscopy.

Our experiment uses ultracold fermionic ^{87}Sr atoms that are nuclear spin-polarized (*17*). We determined the nuclear spin purity of the atomic sample to be greater than 97%. An ultranarrow optical clock transition, whose absolute frequency has been precisely measured (*19*), exists between the ground $^1S_0$ ($|g\rangle$) and excited metastable $^3P_0$ ($|e\rangle$) states. Atoms are trapped in a deep 2D optical lattice at the magic wavelength where the ac Stark shifts of $|g\rangle$ and $|e\rangle$ are matched (*20*). The 2D lattice provides strong confinement along two directions ($\hat{X}$ and $\hat{Y}$) and relatively weak confinement along the remaining dimension ($\hat{Z}$). Using Doppler and sideband spectroscopy, we determined that the lattice-confined atoms are sufficiently cold ($T_X \approx T_Y \approx 2$ μK) that they primarily occupy the ground state of the potentials along the tightly confined directions, with trap frequencies $\omega_X/2\pi \approx 75$ to 100 kHz and $\omega_Y/2\pi \approx 45$ to 65 kHz. This creates a 2D array of isolated tube-shaped potentials oriented along $\hat{Z}$, which have trap frequencies $\omega_Z/2\pi \approx 0.55$ to 0.75 kHz. We estimate that 20 to 30% of the populated lattice sites are occupied by more than one atom. At a typical axial temperature T_Z of a few μK, various axial vibrational modes n are populated in each tube. In our clock experiment, the $|g\rangle \rightarrow |e\rangle$ transition is interrogated via Rabi spectroscopy with the use of a narrow-linewidth laser propagating along $\hat{Y}$. The clock laser and both lattice beams are linearly polarized along $\hat{Z}$. As described in (*10*, *21*), any small projection of the probe beam along $\hat{Z}$ leads to a slightly different Rabi frequency Ω_n for each mode $\Omega_n(\eta_Z^2)$, where $\eta_Z = k_Z a_{ho}/\sqrt{2}$ is the Lamb-Dicke parameter and k_Z represents a small component of the probe laser wave vector along $\hat{Z}$, resulting in a typical $\eta_Z \approx 0.05$.

Spectroscopy of the clock transition is performed with an 80-ms pulse, resulting in a Fourier-limited linewidth of ~10 Hz. The laser power is adjusted to produce a π-pulse on resonance, and the clock laser is locked to the atomic resonance by probing two points on either side of the resonance, with a frequency separation corresponding to the resonance full width at half maximum. The high-finesse Fabry-Perot cavity (*22*) used to narrow the clock laser's linewidth is sufficiently stable over short time scales that it can be used as a frequency reference in a differential measurement scheme (*23*). A single experimental cycle (e.g., cooling and trapping atoms, preparing

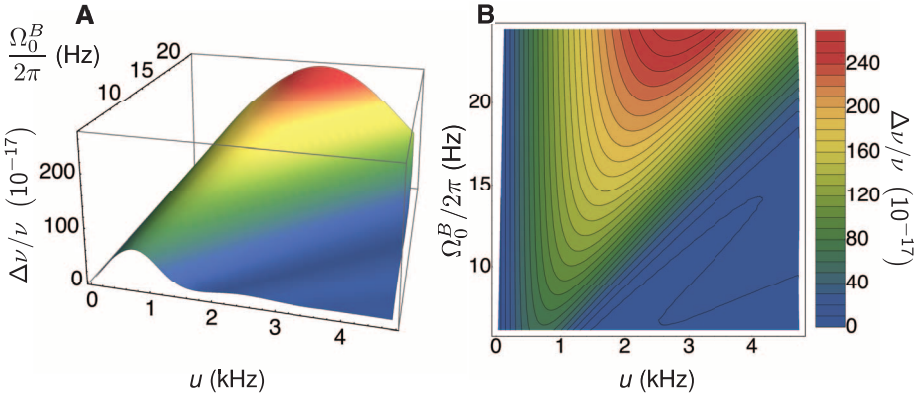

Fig. 2. (**A** and **B**) Three-dimensional plot (A) and contour plot (B) of the calculated suppression of the collisional frequency shift (expressed as a fraction of the transition frequency) with sufficiently large atomic interactions. The criterion for suppression of the collisional shift is $u >> \Omega_0^B$. As Ω_0^B increases, a larger u is required for clock shift suppression. Here the temperature along $\hat{Z}$ was set to $T_Z = 6.5$ μK.

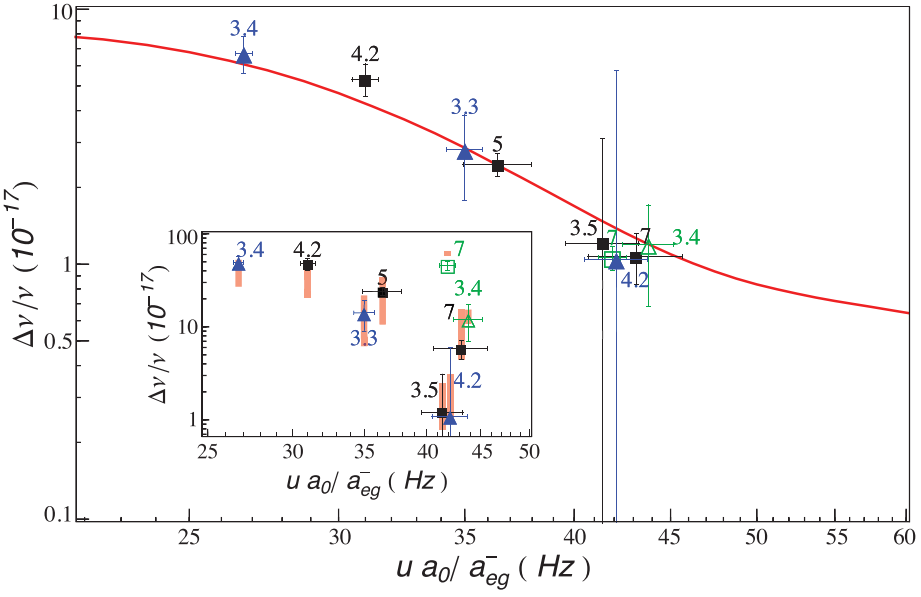

Fig. 3. Experimental observation of the suppression of the collisional frequency shift with increasing interaction energy u. We scale $u = 4\omega_\perp(a_{eg}^-/a_{ho})$ by a_0/a_{eg}^-, where a_0 is the Bohr radius. We varied three important parameters: I_X, T_Z, and Ω_0^B. To better compare the shift at different experimental conditions, we rescale the experimental data by a factor $\Delta\nu^T(\omega_Z^{fix}, T_Z^{fix}, u, \Omega_0^{Bfix})/\Delta\nu^T(\omega_Z^i, T_Z^i, u, \Omega_0^{Bi})$, with $\omega_Z^{fix} = 2\pi \times 0.7$ kHz, $T_Z^{fix} = 4.2$ μK, and $\Omega_0^{Bfix} = \Omega_0^B$. Values of $\Delta\nu^T(\omega_Z^i, T_Z^i, u, \Omega_0^{Bi})$ are calculated using the spin model for $N = 2$ with actual experimental parameters and an effective scattering length of $|a_{eg}^-| = (35$ to $50)a_0$ (see inset). The calculations are scaled by the fraction of the atomic population in doubly occupied lattice sites. A theoretical curve of $\Delta\nu^T(\omega_Z^{fix}, T_Z^{fix}, u, \Omega_0^{Bfix})$ is shown with a solid red line at $|a_{eg}^-| = 40_{a_0}$. The inset shows unscaled experimental data with T_Z indicated for each point. The black and blue symbols were taken at Ω_0^B; the green symbols were taken at $2\Omega_0^B$ and half the interrogation time. Squares and triangles distinguish between two sets of data points measured under different lattice configurations. The vertical extent of the pink rectangles indicates the corresponding spin model predictions for the range of $|a_{eg}^-| = (35$ to $50)a_0$. The variation of ω_Z and u with I_X was explicitly taken into account in the theoretical calculation, which used $\eta_Z = 0.046$ and $\omega_Z = 2\pi \times 0.7$ kHz at the point with the smallest collisional shift.

the 2D lattice, and interrogating the clock transition) requires about 1.5 s, and we modulate the sample density every two cycles. The corresponding modulation of the atomic resonance frequency relative to the cavity reference is a measurement of the density shift.

We performed measurements at several trap depths to directly observe the interaction-induced suppression of the collisional frequency shift. To access different interaction energies, we varied the intensity of the horizontal lattice beam (I_X), which resulted in changed values mainly for ω_X but also for ω_Y and ω_Z. The change in ω_Y arises from the fact that the laser beams that create the two lattices are not orthogonal but instead meet at an angle of 71°. The change in ω_Z results from the Gaussian profile of the beams. Because $u \propto \sqrt{\omega_X \omega_Y \omega_Z}$, an increase of the horizontal beam power leads to a monotonic increase of u. We observe a significant decrease of the collisional shift with increasing horizontal lattice power, as shown by the data points (solid black squares and blue triangles) in Fig. 3 (inset); squares and triangles indicate data taken with slightly different beam waists. We have also studied the dependence of the collisional shift on the Rabi frequency used to drive the clock transition. Ω_0^B was increased by a factor of 2 and the interrogation time was decreased by a factor of 2, yielding a constant Rabi pulse area. Under these conditions, we observed that the collisional shift under similar temperature and trapping conditions increases sharply (green open square and green open triangle in Fig. 3, inset), which confirms that the shift suppression mechanism will not operate effectively for short, higher Rabi-frequency pulses.

In (*17*), we accounted for the combined effects of tunneling, energy offset between wells, and interactions and estimated a fractional error due to tunneling on the order of 1%. Also shown in the inset of Fig. 3 is the shift predicted by the spin model, assuming two atoms per lattice site. The theoretical points are scaled by the fraction of the atomic population in doubly occupied lattice sites. The pink rectangles are the theory results, $\Delta\nu^T(\omega_Z^i, T_Z^i, u, \Omega_0^{Bi})$ with $i = 1, \ldots, 9$, obtained at different temperatures, trapping frequencies, and Rabi frequencies corresponding to the actual experimental conditions under which the data were taken. The spread of theory results (indicated by the vertical extent of the pink rectangles) corresponds to a range of effective scattering lengths $a_{eg}^- = -(35 \text{ to } 50)a_0$ (where a_0 is the Bohr radius). Here we neglect the variation of trap depths across lattice sites (*17*) by assuming that all sites are equivalent to those at the center; the true magnitude of a_{eg}^- is therefore larger than these effective values.

Because the temperature and trapping conditions substantially varied for different experimental data points, some scaling is required to make direct comparisons between the data in Fig. 3 (inset) and the behavior predicted in Fig. 2. To aid visualization of the experimental confirmation of the interaction suppression mechanism, we rescaled the experimentally measured shift values by a factor $\Delta\nu^T(\omega_Z^{\text{fix}}, T_Z^{\text{fix}}, u, \Omega_0^{B\text{fix}})/\Delta\nu^T(\omega_Z^i, T_Z^i, u, \Omega_0^{Bi})$, which is extracted from the theoretical model. Figure 3 shows that after rescaling, all data points lie very close to the theoretical curve of fractional frequency shift versus u at constant $\omega_Z^{\text{fix}} = 2\pi \times 0.7$ kHz, $T_Z^{\text{fix}} = 3.5$ μK, and $\Omega_0^{B\text{fix}} = \Omega_0^B$. The data confirm three important features of the theoretical prediction: (i) The collisional shift Δν decreases with increasing u at similar T_Z and trapping conditions, (ii) Δν increases with increasing Ω_0^B at similar T_Z and trapping conditions, and (iii) Δν decreases with smaller T_Z. The sign of the observed shift is negative (i.e., an increased sample density shifts the atomic resonance to lower frequencies). Previous studies of the collisional shift in a 1D optical lattice (*8*, *10*) are consistent with this observation. From the present data set, we can unambiguously conclude that a_{eg}^- is negative.

We have made an extensive series of collisional shift measurements at the largest trap depths available to us (Fig. 4). The free-running clock laser has a stability of ~1.5×10^{-15} at time scales of 1 to 10 s (*22*). Therefore, a substantial integration time is required to determine the collisional shift with an uncertainty of 10^{-17}. Frequency drifts are minimized by measuring the long-term drift in the resonance frequency (relative to the ultrastable reference cavity) and applying a feedforward correction to the clock laser. The correlation between the atomic resonance frequencies and the density of trapped atoms was calculated by analyzing overlapping sequences of four consecutive measurements and eliminating frequency drifts of up to second order (*24*). Approximately 60 hours of data were acquired at $T_Z = 7$ μK over a ~2-month time period for the record shown in Fig. 4A. Each data point represents a period during which the clock was continuously locked, with error bars

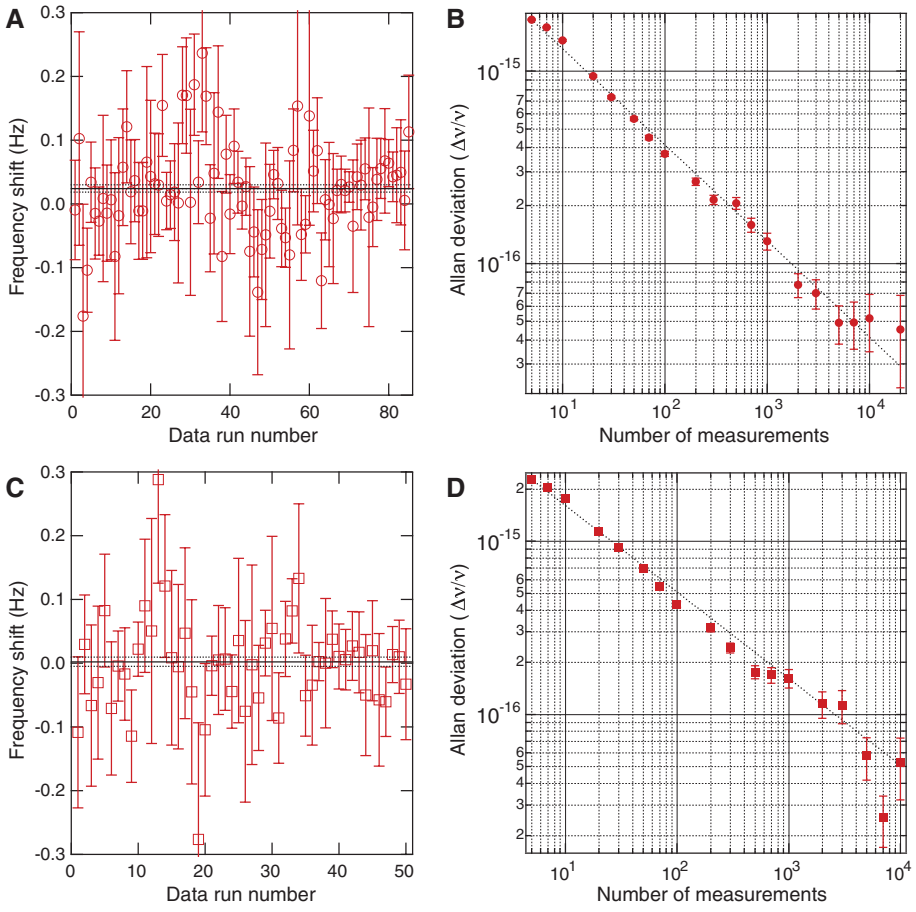

Fig. 4. (**A** to **D**) Data records of collision-induced frequency shift measurements for ^{87}Sr atoms confined in a 2D optical lattice. Each point represents a data set collected from a continuous operation of the Sr clock, with error bars determined from the SE of that data set. The weighted mean and weighted error of all the data are determined from the shift and error values of each data set, and the weighted error is scaled by the square root of the reduced χ^2, $\sqrt{\chi^2_{\text{red}}}$. These are shown as the solid and dashed horizontal lines in (A) and (C). Shown in (B) and (D) are the corresponding Allan deviations (ignoring dead time between data runs) of the frequency shift records displayed in (A) and (C), respectively. Each measurement represents a differential comparison between two density conditions. Under typical clock operating conditions ($N \approx 2000$), the weighted means and SEs of the fractional frequency shift are $5.6\ (\pm 1.3) \times 10^{-17}$ at $T_Z = 7$ μK [(A) and (B)] and $0.5\ (\pm 1.7) \times 10^{-17}$ at $T_Z = 3.5$ μK [(C) and (D)]. For the 7-μK data, the reduced χ^2 was $\sqrt{\chi^2_{\text{red}}} = 0.84$, and for the 3.5-μK data $\sqrt{\chi^2_{\text{red}}} = 0.73$.

determined from the standard error of the measurements in that data set (*17*). At an axial temperature $T_Z \approx 7$ μK, the collisional shift in our 2D lattice clock was measured to be 5.6 (±1.3) × 10^{-17} in fractional units, with $\sqrt{\chi^2_{red}} \approx 0.84$. At a lower T_Z of 3.5 μK, the collisional shift is reduced to 0.5 (±1.7) × 10^{-17}, with $\sqrt{\chi^2_{red}} \approx 0.73$ (Fig. 4C). The corresponding Allan deviations of both data sets are shown in Fig. 4, B and D.

Relative to previous measurements of collisional shifts in a 1D optical lattice (*8*, *10*), the atomic density in our 2D lattice is an order of magnitude higher. Hence, given a similar level of excitation inhomogeneity, if the collisional shift in a 2D lattice were not suppressed, we would expect a larger shift than seen in earlier results, even after accounting for the fact that only 20 to 30% of lattice sites are contributing.

The advance presented here removes an important obstacle to further increasing the precision and accuracy of neutral atom–based optical clocks. Increasing the number of atoms loaded into our 2D lattice system will enable us to improve the stability of our clock without imposing an onerous systematic effect. As clock lasers become more stable, we will increase the duration of the Rabi interrogation pulse, thus decreasing the Rabi frequency, further reducing the collisional shift systematic well into the 10^{-18} domain. This, together with the fact that in the strongly interacting regime the collisional shift will remain suppressed (*25*) as more atoms are loaded into individual lattice sites, should enable neutral atom clocks to operate with the large sample sizes needed to achieve the highest possible stability.

References and Notes

1. S. Gupta *et al.*, *Science* **300**, 1723 (2003).
2. M. Punk, W. Zwerger, *Phys. Rev. Lett.* **99**, 170404 (2007).
3. G. Baym, C. J. Pethick, Z. Yu, M. W. Zwierlein, *Phys. Rev. Lett.* **99**, 190407 (2007).
4. M. Girardeau, *J. Math. Phys.* **1**, 516 (1960).
5. T. Kinoshita, T. Wenger, D. S. Weiss, *Science* **305**, 1125 (2004).
6. B. Paredes *et al.*, *Nature* **429**, 277 (2004).
7. E. Haller *et al.*, *Science* **325**, 1224 (2009).
8. A. D. Ludlow *et al.*, *Science* **319**, 1805 (2008).
9. M. D. Swallows *et al.*, *IEEE Trans. Ultrason. Ferroelectr. Freq. Control* **57**, 574 (2010).
10. G. K. Campbell *et al.*, *Science* **324**, 360 (2009).
11. N. D. Lemke *et al.*, *Phys. Rev. Lett.* **103**, 063001 (2009).
12. K. Gibble, *Phys. Rev. Lett.* **103**, 113202 (2009).
13. A. M. Rey, A. V. Gorshkov, C. Rubbo, *Phys. Rev. Lett.* **103**, 260402 (2009).
14. Z. Yu, C. J. Pethick, *Phys. Rev. Lett.* **104**, 010801 (2010).
15. M. M. Boyd *et al.*, *Phys. Rev. A* **76**, 022510 (2007).
16. T. Akatsuka, M. Takamoto, H. Katori, *Nat. Phys.* **4**, 954 (2008).
17. See supporting material on *Science* Online.
18. M. Saffman, T. G. Walker, K. Molmer, *Rev. Mod. Phys.* **82**, 2313 (2010).
19. G. K. Campbell *et al.*, *Metrologia* **45**, 539 (2008).
20. J. Ye, H. J. Kimble, H. Katori, *Science* **320**, 1734 (2008).
21. S. Blatt *et al.*, *Phys. Rev. A* **80**, 052703 (2009).
22. A. D. Ludlow *et al.*, *Opt. Lett.* **32**, 641 (2007).
23. M. M. Boyd *et al.*, *Phys. Rev. Lett.* **98**, 083002 (2007).
24. W. B. Dress, P. D. Miller, J. M. Pendlebury, P. Perrin, N. F. Ramsey, *Phys. Rev. D* **15**, 9 (1977).
25. We recently became aware of a conference proceedings report that contains a brief discussion on suppression of collisional shifts under strong interactions (*26*).
26. K. Gibble, www.ieee-uffc.org/main/publications/fcs/toc.asp?year=2010.

27. We thank C. Benko for technical assistance, and A. D. Ludlow and A. Gorshkov for useful discussions. Supported by a National Research Council postdoctoral fellowship (M.D.S.), a National Defense Science and Engineering Graduate fellowship (M.B.), and a grant from the Army Research Office with funding from the Defense Advanced Research Projects Agency OLE program, the National Institute of Standards and Technology, the NSF Physics Frontier Center at JILA, and the Air Force Office of Scientific Research.

Supporting Online Material

www.sciencemag.org/cgi/content/full/science.1196442/DC1
Materials and Methods
Figs. S1 to S4
References

12 August 2010; accepted 20 January 2011
Published online 3 February 2011;
10.1126/science.1196442

Direct Measurement of Long-Range Third-Order Coherence in Bose-Einstein Condensates

S. S. Hodgman, R. G. Dall, A. G. Manning, K. G. H. Baldwin, A. G. Truscott*

A major advance in understanding the behavior of light was to describe the coherence of a light source by using correlation functions that define the spatio-temporal relationship between pairs and larger groups of photons. Correlations are also a fundamental property of matter. We performed simultaneous measurement of the second- and third-order correlation functions for atoms. Atom bunching in the arrival time for pairs and triplets of thermal atoms just above the Bose-Einstein condensation (BEC) temperature was observed. At lower temperatures, we demonstrated conclusively the long-range coherence of the BEC for correlation functions to third order, which supports the prediction that like coherent light, a BEC possesses long-range coherence to all orders.

The interchangeability of particle and wave-like behavior is fundamental to the quantum-mechanical description of light, but not until the seminal work of Glauber (*1*) was quantum theory used to provide a description of the coherence properties of photon statistics that moves beyond classical theory. That work distinguishes between the classical, first-order coherence of the light intensity and the quantum coherence between *n* multiple photons (*n*th-order correlations); a perfectly coherent source exhibits coherence to all orders. For example, measurement of the arrival time of individual photons at a detector enables the correlation between pairs (second-order), triplets (third-order), and higher-order groups of photons to be determined. An incoherent source of light will exhibit bosonic photon bunching—that is, an enhanced probability of pairs of photons arriving within an interval that defines the coherence time of the source. Such second-order correlations were first demonstrated in the famous Hanbury Brown and Twiss (HBT) experiment (*2*), a technique that was later applied in astronomy in the spatial domain to determine the angular size of stars (*3*). Conversely, a highly coherent light source such as a laser will exhibit no bunching, with a uniform arrival-time probability for pairs, triplets, and larger groupings of photons; this indicates long-range coherence to all orders in the corresponding (unity-value) correlation functions.

The same concepts can be applied to the quantum statistics of matter, with correlations demonstrated in systems ranging from nuclear collisions (*4*) to free electrons (*5*) to neutrons (*6*). In atomic physics, correlations can potentially be probed by using spin polarization spectroscopy (*7*, *8*), spin-squeezing entanglement (*9*, *10*), and interactions between atoms in single-occupancy optical lattices (*11*). Specifically, incoherent sources of bosonic atoms have also been shown to exhibit HBT-like (second-order) bunching behavior (*12*, *13*), whereas incoherent fermionic sources exhibit anti-bunching (a reduced probability of particles being found close together) (*14*, *15*) as a consequence of the Pauli exclusion principle. However, correlations higher than second order are often difficult to measure because the vast amounts of data require extensive data analysis resources. Correlations up to third order have been measured for exciton-polaritons (*16*) and to fourth order for photons (*17*).

First-order (*18*) and second-order correlations (*12*–*15*, *19*–*22*) have been measured for atomic matter waves, and the effect of second- and third-order correlations on two-body (*23*) and three-body (*24*, *25*) loss rates has been demonstrated. In order to prove that an atomic ensemble is completely quantum coherent, it is necessary to demonstrate coherence in the third (and subsequent) orders (*1*). Measurements of third- and higher-order correlations are also important in order to understand whether the interactions between atoms (not present for photons) affect the coherence of matter-wave sources, such as Bose-Einstein condensates (BECs). Intrinsically, higher-order (*n* body) correlation functions are a

Australian Research Council Centre of Excellence for Quantum Atom Optics, Research School of Physics and Engineering, Australian National University, Canberra, ACT 0200, Australia.

*To whom correspondence should be addressed. E-mail: andrew.truscott@anu.edu.au